Title
HEAVY TARGET FRAGMENTATION AND THE ENERGY DEPENDENCE OF NUCLEUS-NUCLEUS TOTAL REACTION CROSS SECTIONS

Author
Laveland, W.

Publication Date
1984

LBL-16931
Preprint

Lawrence Berkeley Laboratory
UNIVERSITY OF CALIFORNIA

Submitted to Zeitschrift für Physik A

HEAVY TARGET FRAGMENTATION AND THE ENERGY DEPENDENCE OF NUCLEUS-NUCLEUS TOTAL REACTION CROSS SECTIONS

W. Loveland, C.P. Oertel, D.J. Morrissey,
P.O. McGaughey, G.T. Seaborg, and K. Aleklett

January 1984

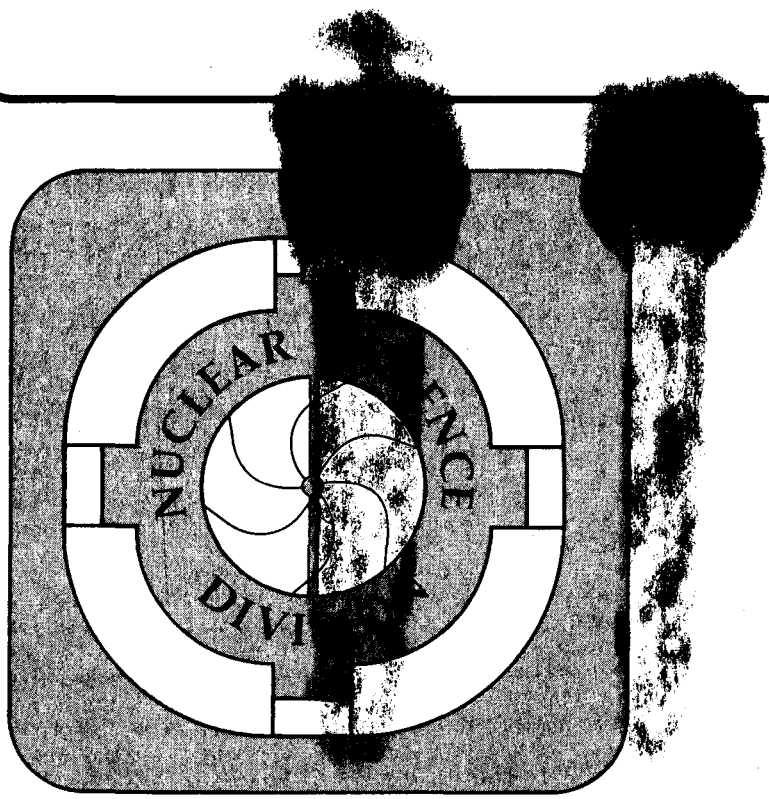

Prepared for the U.S. Department of Energy under Contract DE-AC03-76SF00098

DISCLAIMER

LBL-16931

HEAVY TARGET FRAGMENTATION AND THE ENERGY DEPENDENCE OF NUCLEUS-NUCLEUS TOTAL REACTION CROSS SECTIONS

W. Loveland, C. P. Oertel*,
Department of Chemistry, Oregon State University
Corvallis, Oregon 97331

D. J. Morrissey
Department of Chemistry, Michigan State University
E. Lansing, Michigan 48824

P. O. McGaughey+, G. T. Seaborg
Nuclear Science Division, Lawrence Berkeley Laboratory
University of California, Berkeley, California 94720

and

K. Aleklett
Studsvik Science Research Laboratory
S-611 82 Nykoping, Sweden

ABSTRACT

The target fragment yield distributions were measured for the interaction of 3.0 and 25.2 GeV ^{12}C and 42.0 GeV ^{20}Ne with ^{181}Ta. From these measurements (and other data), lower limits on the total reaction cross sections $\sigma_R^<$ were derived for the ^{20}Ne + ^{181}Ta reaction for projectile energies from 7-2100 MeV/u. These values of $\sigma_R^<$ are best described in terms of a dip in $\sigma_R^<$ near 200-400 MeV/u although they are consistent with an invariant value of $\sigma_R^<$ from 17 - 2100 MeV/u. The data are compared with predictions of the total reaction cross section $\sigma_R^<$, of nucleus-nucleus optical models and seem to be in general agreement with these predictions.

I. Introduction

In recent years, considerable interest has been expressed in the energy dependence of nucleus-nucleus total reaction cross sections. In the seminal papers of DeVries and Peng [1,2] they suggested that nucleon-nucleon interactions dominate nucleus-nucleus collisions at intermediate as well as high energies. The well-known decrease in the nucleon-nucleon scattering cross section for energies of 10 - 200 MeV is thus predicted to cause the nucleus-nucleus total reaction cross section to drop as the projectile energy per nucleon exceeds a few tens of MeV. Available data for light ion-(light/medium mass targets) was shown to be in agreement with these ideas. Similar behavior was also predicted (and found) for nucleus-nucleus total cross sections [3]. This decrease in the cross section wth increasing projectile energy can be parameterized as

$$\sigma_R = (R + \lambda\!\!\!^{-})^2 \quad (1 - T\,[E]) \quad 1 - \left(\frac{zZe^2}{(R + \lambda\!\!\!^{-})\,E} \right) \qquad (1)$$

where R is the effective nuclear radius, $\lambda\!\!\!^{-}$ is the reduced wave length of the incident particle, Z and z refer to the target and projectile, respectively, E is the center of mass energy, and T [E] is the energy dependent transparency. Microscopic calculations showed that non-zero transparencies at medium energies arose from collisions with large impact parameters involving a "translucent" region of surface nucleons.

The hypotheses advanced by DeVries and Peng raise fundamental questions affecting issues such as the viability of hydrodynamic descriptions of intermediate energy heavy ion reactions. In view of the importance (indicated by microscopic calculations) of surface interactions in determining the transparency in nucleus-nucleus total reaction cross sections, we thought it would be interesting to consider the behavior of the

total reaction cross section, σ_R, as a function of projectile energy in heavy ion - heavy target reactions where significant portions of the cross section do not involve surface interactions.

Little published data about the energy variation of σ_R for heavy ion - heavy target reactions for intermediate and high energies exist. Buenerd et al. [4] did study the elastic scattering of 86 MeV/A ^{12}C from ^{208}Pb and deduced a T value of 0.42 from an optical model analysis of the data. Grabez et al. [5] in a track detector study of the same reaction measured a lower limit for σ_R which was 27% larger than the value of σ_R measured by Buenerd et al. To avoid discrepancies such as this, (which may be more apparent than real due to the different experimental techniques used) and to study the general variation of the total reaction cross section with projectile energy, it would be valuable to have a series of measurements at different projectile energies using the same experimental technique.

While such data are not available, we believe an interesting series of measurements does exist which can give us insight into the question of the general variation of σ_R with projectile energy. The data we have in mind are the measured target fragment yield distributions from heavy ion-heavy nucleus reactions. Such yield distributions usually include the yields of target fragments with $24 \leq A \leq A_{tgt}$ which generally account for $\geq$ 85% of the geometric cross section. Strictly speaking, of course, such distributions give a lower limit on the total reaction cross section due to the exclusion of processes such as total nuclear breakup or inelastic events in which the target nucleus de-excites without particle emission, etc. However, the data may contain global features of the energy dependence of the nucleus-nucleus cross section. In this paper we gather together the results of several earlier measurements of target fragment yield distributions made by us, present a limited amount of new data on yield

distributions in the interaction of 250 MeV/u ^{12}C, 2.1 GeV/u ^{12}C, and 2.1 GeV/u ^{20}Ne with ^{18}Ta, and summarize the results concerning the energy variation (and magnitude) of this lower limit on the total reaction cross section, $\sigma_R^<$. The results show a general invariance of, or only small changes in, $\sigma_R^<$ for projectile energies of 10 MeV/u to 2.1 GeV/u, and are compared to microscopic calculations.

II. Experimental

As stated above, we wish to present new results of measurements of the target fragment yield distributions in the reaction of 3.0 GeV ^{12}C, 25.2 GeV ^{12}C and 42.0 GeV ^{20}Ne with ^{181}Ta. The measurements used the irradiation facilities of the LBL Bevalac. Tantalum metal targets of thickness 86.8, 248 and 86.8 mg/cm^2 surrounded by mylar catcher foils of thickness 36 mg/cm^2 were irradiated with 3.0 GeV ^{12}C, 25.2 GeV ^{12}C and 41.0 GeV ^{20}Ne, respectively, for periods of 1605, 802 and 545 min. The average particle fluxes were 5.22 x 10^{10}, 2.87 x 10^{10}, and 3.51 x 10^9 particles/ min. respectively, for the three bombardments.

Assay of the radioactivities of the target fragments that stopped in the target and catcher foils by γ-ray spectroscopy began approximately one hour after the end of the irradiation and continued for approximately two months. Standard techniques that have been described elsewhere [6] were used to identify the radionuclides present and to determine their activities. No corrections for the effect of secondary induced reactions were made because previous studies [7] of heavy ion - Au collisions at similar energies showed such corrections to be negligible. In these studies [7], the production of 23 different target fragments ($46 \leq A \leq 196$) in the reaction of 8.0 GeV ^{20}Ne with ^{197}Au was measured for 242 and 49.3 mg/cm^2 targets. No difference was observed in the production cross sections for the two target thicknesses indicating negligible contributions

of secondary reactions.

The measured radionuclide production cross sections are given in Tables I, II and III. Fifty-three different radionuclides were observed for the reaction of 3.0 GeV ^{12}C with ^{181}Ta while 52 and 36 nuclides were observed in the reaction of 25.2 GeV ^{12}C and 42.0 GeV ^{20}Ne, respectively with ^{181}Ta.

The radionuclide production cross sections, as stated previously, include both independent yields and partial cumulative yields. To obtain true independent yield cross sections for all the species, one needs to correct the partial cumulative yield cross sections for the effects of any beta decay that occured between the time of production and the time of detection of a particular species. Once this correction has been made, the resulting independent yield production cross sections represent the yield of a target fragment of given mass and atomic number and can be integrated to give the total yield of a given A or Z in the reaction as well as the total cross section for target residue production.

In order to make the correction for precursor decay to each measured partial cumulative yield cross section and in order to calculate the total isobaric or mass yield we have assumed that the independent yields of isobars can be represented by a histogram that lies along a Gaussian curve as given by equation (1).

$$\sigma(Z,A) = \sigma(A) \left\{ 2\pi s_z{}^2(A))^{-1/2} \exp\left[\frac{(Z - Z_p(A))^2}{-2s_z{}^2(A)} \right] \right\} \qquad (2)$$

with $\sigma(A)$ being the total isobaric yield, $s_Z(A)$, the Gaussian width parameter, and $Z_p(A)$ the most probable Z value for that isobar. Given the

assumption of Gaussian atomic number dispersions, the beta decay feeding correction factors for cumulative yield isobaric members can be calculated once the centroid and width of the Gaussian are known.

In order to uniquely specify these three variables $\sigma(A)$, $s_z(A)$ and $Z_p(A)$ one would need to measure three independent yield cross sections for each isobar. In fact, the nature of radiochemical studies such as this one does not, in general, lend itself to the measurement of the yields of different isobars. Rather, a wide assortment of radioactivities are observed which span the entire range of the periodic table that is accessible in the nuclear reaction. As a result relatively few isobaric pairs are observed making a further assumption necessary to apply the Gaussian charge distributions to the measured data. The assumption is, that the value of $\sigma(A)$ varies smoothly and slowly as a function of mass number, A, and is roughly constant within any A range considered when determining Zp(A) and $s_z(A)$. Another less stringent statement of the assumption is that the charge dispersion curves for neighboring isobaric chains should be similar, thus, radionuclide yields from a limited mass range can be used to determine a single charge dispersion curve. The two parameters that specify the width, $s_z(A)$, and the center Zp(A), of the Gaussian distributions are varied in an iterative fit to the measured data over limited mass regions. The width parameter has been found, in general, to be approximately independent of mass number over small ranges of A. The centers of the distributions were adequately represented by linear functions in A, over small ranges of A.

The results of this procedure can be seen in Fig. 1-3, where the calculated independent yield production cross sections are plotted versus $Z - Z_p(A)$, the distance in Z units from the center of the isobaric distribution. Also shown in Figs 1-3 are the Gaussian curves that are

specified by equation (2). The yields of isomers are denoted by triangles in Fig. 1-3.

The uncertainties in the calculated independent yields represent the contribution from statistical uncertainties in the measurements and an arbitrary factor representing the minimum systematic uncertainty in each data point of 10% where applied. [8] The variation of the parameter $Z_p(A)$ (which specified the center of the charge distributions) with product mass number A is shown in Figure 4 for the systems studied. In general the Zp functions are quite similar for the three systems with small differences appearing for near-target spallation products. The data of Figs. 1-3 and the parameters of the Gaussian distributions can be used to calculate a total isobaric yield for each data point. [7] These isobaric yields are shown in Fig. 5 and are also given in Tables I-III. In cases where the yield of one member of an isomeric pair did not represent adequately the yield of both members of that pair, no isobaric yield was calculated. When calculated independent yields for two isobars exist, the resulting mass yields were added to give the final mass yield for that isobar.

The uncertainties in each point in Fig. 5 simply represent the fractional uncertainty in the calculated independent yield and not any systematic uncertainty introduced by the charge dispersion analysis. The magnitude of this latter uncertainty depends on the extent to which each independent radionuclide yield is well described by a Gaussian charge distribution, the position of the measured radionuclide Z relative to Zp, uncertainties in Zp(A) and $s_z(A)$ and the extent to which the mass yield curve is a slow, smoothly varying function of A whose magnitude and shape is to be determined. Morrissey et al. [7] have suggested one can estimate by using a propagation of errors treatment that on the average, individual points in the isobaric yield distribution have a systematic uncertainty of

± 30% which should be added quadratically to the uncertainty in the measured value. However, they estimate the average isobaric yield within each small A region is known to ± 15%.

III. Results and Discussion

In order to integrate the data of Fig. 5 (and similar data for other projectile energies) to give values of the total "residue" cross section $\sigma_R^<$, certain assumptions need to be made. First, we assume that with the exception of fission fragments, the multiplicity of all fragments with $A \geq 60$ is unity. (We can correct for the effects of fission [multiplicity = 2] using published values of the fission cross section or by assuming that all fragments contributing to any central "bump" in the mass yield curve [especially at low and intermediate projectile energies] are fission fragments.) For fragments with $A > A_{tgt}/2$, this assumption of unit multiplicity for non-fission fragments is obviously valid. The yields of such fragments typically amount to ~75% of the geometrical reaction cross section. For fragments with $60 \leq A \leq A_{tgt}/2$ it is numerically possible to have fragment multiplicities of 2 or more. However, studies [9] of such processes in the reaction of 11.5 GeV protons with ^{238}U have shown these binary reactions are rare. We do not choose to integrate the yields below A = 60 because the work of Warwick et al. [10] showed large multiplicities of A = 20 - 40 fragments in relativistic nuclear collisions.

In Table IV, we show the total "residue" cross section for the three reactions described in this work and for all the reactions involving Au and Ta target nuclei that we have measured. [11, 12] We also show results derived from the isobaric yield data of Kaufman et al. [19] for the reaction of 4.8 GeV ^{12}C + ^{197}Au. In this radiochemical work, a somewhat different approach to integrating the measured nuclidic cross sections to give isobaric yields was taken. It is gratifying to note the agreement

between our data and that of Kaufman et al. In all cases we show the total integrated cross section for $A \geq 60$, the correction for fission and how it was estimated and the resulting total "residue" cross section. To compare these data from several different projectile - target systems, we have assumed that for a given projectile energy per nucleon (in the c.m. system), that the Z, A dependence of the cross sections is that given by the soft spheres model. [13] Thus to convert the cross section for the $^{12}C+^{197}Au$ reaction at a c.m. projectile energy of χ MeV/A to a value appropriate for the $^{20}Ne + ^{181}Ta$ reaction at the same c.m. projectile energy of χ MeV/A, we simply multiply it by the ratio of the soft spheres cross sections for the reactions in question at χ MeV/u. This use of the soft spheres cross sections for Z, A scaling is consistent with projectile fragmentation data. [14] All the data for the cases tabulated in Table IV has been converted to values appropriate to the $^{20}Ne + ^{181}Ta$ reaction and plotted in Fig. 6. Despite earlier caveats about comparing data gathered using different experimental techniques we also show in Fig. 6 (after appropriate conversion) the data of Buenerd et al. [4], Grabez et al. [5], and Videbaek et al. [15]

Certain features of Fig. 6 deserve further comment. At a projectile energy (lab) of 86 MeV/A, the results of three measurements are shown. They are the lower limit on σ_R as measured using track detectors by Grabez et al. [5], the lower limit on σ_R deduced from radiochemical data [11] and the true value of σ_R as deduced by optical model analysis of elastic scattering. [4] What is interesting is that the two values of $\sigma_R^<$ are the same within experimental uncertainty as the value of σ_R indicating the $\sigma_R - \sigma_R^<$ is not large at this energy. At a projectile energy of 2.1 GeV/A, there is some disagreement between the two radiochemical measurements although both measurements lie within two standard deviations of the mean of

the two measurements. The average deviation of $\sigma_R^<$ from the value of σ_R predicted by the soft spheres model [13] is ∿12% for the energy region from 45-2100 MeV/A again indicating that $\sigma_R - \sigma_R^<$ is small. The data are consistent with an invariant value of $\sigma_R^<$ from 15-2100 MeV/A but are better described by a dip in $\sigma_R^<$ in the region of 100-400 MeV/A. (A Student's t-test would indicate that the mean of the data points at 235, 360, and 377 MeV/A is statistically significantly different [5% rejection level] from the mean of the other data points from 17-2100 MeV/u.)

It is interesting to compare the observed energy dependence of $\sigma_R^<$ with theoretical expectations for σ_R. In Fig. 6, we also show the energy dependence of the true $^{20}Ne + {}^{181}Ta$ total reaction cross section as predicted by the microscopic theory of DeVries and Peng. [2] These microscopic calculations, based on Glauber theory, predict that the transparency in nucleus-nucleus collisions is due to a large impact parameter "translucent" region, corresponding to interactions involving the surface regions of the colliding nuclei. With a heavy nucleus such as Ta, most collisions involve the central densities of projectile and target. Thus transparency effects are predicted to be small. Indeed, the calculations predict a generally invariant value of σ_R from 20-2100 MeV/A with a very small dip in σ_R near 100-400 MeV/A.

We also show in Fig. 6 the values of σ_R predicted by a high energy double folding optical potential approximation by Townsend et al. [16] who say it is more accurate than the DeVries and Peng calculation. The predicted values of σ_R are considerably less than those of DeVries and Peng and show a decrease in σ_R from 50-500 MeV/A. The significance of the agreement between the predictions of Ref. 16 and the magnitude of $\sigma_R^<$ is difficult to assess. Normally one would expect $\sigma_R^<$ to be somewhat less than σ_R and the agreement between the predicted value of σ_R and the

measured value of $\sigma_R^<$ would indicate a problem. However, the situation is clouded by the agreement between two measurements of $\sigma_R^<$ at 86 MeV/A and the measurement of σ_R by Buenerd et al.

The comparison of the data with the theoretical predictions is both interesting and frustrating. The $\sigma_R^<$ data lie considerably below the DeVries and Peng predictions for projectile energies of 7-20 MeV/A presumably because the values of $\sigma_R^<$ do not include contributions from quasielastic events whose importance is greatest at lower energies. The data points in Figure 6 are less than the predictions of the DeVries and Peng calculations but that is expected since these are lower limits on σ_R. The calculations of Ref. 16 describe the data from 50-2100 MeV/u adequately except for the previously noted fact that $\sigma_R^<$ should be a lower limit on σ_R and not be the true value of σ_R. The best fit to the values of $\sigma_R^<$ would indicate a dip (in the energy region of 100-500 MeV/u) whose magnitude is greater than predicted, but in better agreement with the calculations of Ref. 16. It would be helpful in comparing the DeVries and Peng calculations and those of Townsend et al [16] to have a series of measurements of absolute values of σ_R.

IV. Summary

What we can infer from the $\sigma_R^<$ data and the theoretical predictions of σ_R? One concludes that

(a) It is possible to use radiochemical target fragment distribution data to study the general features of the energy variation of σ_R. These lower limit reaction cross sections, $\sigma_R^<$ agree with other measurements and indicate that $\sigma_R - \sigma_R^<$ is small. Systematic undertainties in the values of $\sigma_R^<$ limit their usefulness in evaluating small differences between theoretical predictions or small changes in σ_R.

(b) While the data are consistent with invariance of $\sigma_R^<$ from 40-2100 MeV/u, they are best described in terms of a small dip in $\sigma_R^<$ in a region near 200-400 MeV/u.

(c) The data are generally consistent with optical model predictions of DeVries and Peng [2] and Townsend et al. [16] with the data being in better agreement with the trend of the Townsend et al. predictions.

V. Acknowledgements

We acknowledge the participation of L. L. Nunnelley in data analysis. We are especially grateful to J.C. Peng for performing the calculations of σ_R using the DeVries and Peng optical model. This work was supported in part by the Director, Office of Energy Research, Division of Nuclear Physics of the Office of High Energy and Nuclear Physics of the U. S. Department of Energy under Contract DE-AC03-76SF00098.

Table I

Product Yields from the Irradiation of 3.0 GeV ^{12}C with ^{181}Ta

Nuclide	Measured Radionuclide Yield (mb)	Isobaric Yield (mb)	Nuclide	Measured Radionuclide Yield (mb)	Isobaric Yield (mb)
^{24}Na	10.2 ± 0.3	12.2 ± 1.3	^{86}Y	5.9 ± 0.6	9.7 ± 1.0
^{28}Mg	2.4 ± 0.1	8.7 ± 0.7	^{87m}Y	8.1 ± 0.4	9.5 ± 0.4
^{44m}Sc	1.2 ± 0.1	___ [a]	^{87}Y	5.9 ± 1.5	7.1 ± 1.8
^{46}Sc	5.3 ± 0.7	7.8 ± 1.0	^{88}Y	4.0 ± 0.5	10.3 ± 1.2
^{48}Sc	1.6 ± 1.0	8.4 ± 5.0	^{89}Zr	6.3 ± 0.2	7.9 ± 0.8
^{52}Mn	0.87 ± 0.16	5.9 ± 1.1	^{93m}Mo	2.6 ± 0.3	___ [a]
^{59}Fe	1.77 ± 0.18	7.9 ± 0.8	^{94}Tc	4.4 ± 0.4	10.5 ± 1.1
^{67}Ga	2.4 ± 0.5	4.9 ± 1.1	^{95}Tc	5.8 ± 0.7	8.7 ± 1.0
^{69}Ge	3.0 ± 0.4	7.4 ± 1.1	^{96}Tc	2.7 ± 0.3	___ [a]
^{73}Se	1.2 ± 0.2	4.5 ± 0.8	^{97}Ru	6.9 ± 0.1	11..6 ± 1.2
^{74}As	2.7 ± 0.1	6.4 ± 0.6	^{101m}Rh	4.3 ± 0.5	___ [a]
^{75}Se	5.2 ± 0.3	6.7 ± 0.7	^{105}Ag	9.0 ± 1.6	10.3 ± 1.8
^{83}Rb	6.9 ± 1.0	11.5 ± 1.7	^{106m}Ag	2.3 ± 0.1	___ [a]

Table I (cont.)

Product Yields from the Irradiation of 3.0 GeV ^{12}C with ^{181}Ta

Nuclide	Measured Radionuclide Yield (mb)	Isobaric Yield (mb)	Nuclide	Measured Radionuclide Yield (mb)	Isobaric Yield (mb)
^{110m}In	3.5 ± 1.9	---[a]	^{145}Eu	25.3 ± 0.7	29.6 ± 3.0
^{111}In	8.9 ± 0.7	10.8 ± 1.1	^{147}Gd	20.1 ± 6.0	29.4 ± 8.7
^{118m}Sb	1.06 ± 0.48	---[a]	^{149}Gd	30.8 ± 1.7	34 ± 3
^{119m}Te	2.0 ± 0.1	---[a]	^{150}Tb	10.0 ± 0.4	---[a]
^{120}I	7.4 ± 2.0	15.7 ± 4.3	^{151}Tb	40.0 ± 8.3	41 ± 9
^{121}Te	12.3 ± 2.3	15.4 ± 2.9	^{152}Tb	24.5 ± 9.9	26 ± 10
^{122}Xe	8.4 ± 2.8	27.0 ± 9.0	^{155}Dy	29.3 ± 3.3	30.1 ± 3.4
^{123}I	19.7 ± 2.5	22.1 ± 2.8	^{165}Tm	36.0 ± 1.0	38.6 ± 3.9
^{125}Xe	12.8 ± 4.7	14.3 ± 5.3	^{169}Lu	42.4 ± 3.5	58 ± 6
^{127}Xe	18.6 ± 0.2	32 ± 3	^{170}Hf	40.7 ± 2.1	66 ± 7
^{127}Cs	14.1 ± 1.3	17 ± 2	^{172}Lu	0.97 ± 0.21	31 ± 7
^{128}Ba	8.7 ± 0.8	17.8 ± 1.8	^{173}Hf	27.4 ± 2.1	35.7 ± 3.6
^{132}La	11.8 ± 2.5	14.6 ± 3.0	^{175}Hf	4.4 ± 0.3	26.6 ± 2.7
^{135}Ce	15.7 ± 0.5	18. ± 2			

a Isobaric yield not determined because yields of both members of isomeric pair not measured

Table II

Product Yields from the Interaction of 25.2 GeV ^{12}C with ^{181}Ta

Nuclide	Measured Radionuclide Yield (mb)	Isobaric Yield (mb)	Nuclide	Measured Radionuclide Yield (mb)	Isobaric Yield (mb)
^{24}Na	33 ± 3	37 ± 4	^{84}Rb	2.2 ± 0.2	7.1 ± 0.7[b]
^{28}Mg	6.7 ± 0.7	20 ± 2	^{86}Y	8 ± 2	14 ± 3[b]
^{42}K	9.2 ± 0.9	14 ± 2	^{87m}Y	12 ± 1	——[a]
^{48}V	3.5 ± 0.7	11 ± 2	^{89}Zr	9.0 ± 0.9	12 ± 2[b]
^{48}Sc	2.2 ± 0.6	12 ± 3	^{93m}Mo	3.6 ± 0.4	——[a]
^{51}Cr	9.3 ± 0.3	16 ± 2	^{94}Tc	5.1 ± 0.5	——[a]
^{52m}Mn	6 ± 5	—[a]	^{96}Tc	3.3 ± 2.6	7.4 ± 5.8[b]
^{56}Mn	8 ± 1	20 ± 3	^{97}Ru	7 ± 1	7.9 ± 0.8
^{56}Co	0.9 ± 0.1	12 ±2	^{101m}Rh	10 ± 3	——[a]
^{58}Co	7.5 ± 0.8	15 ± 2[b]	^{105}Ag	10 ± 1	11 ± 1[b]
^{59}Fe	2.3 ± 0.2	13 ± 2	^{110m}In	10 ± 2	——[a]
^{60}Co	5.5 ± 0.6	12 ± 2[b]	^{111}In	9.3 ± 0.4	9.5 ± 0.9[b]
^{69}Ge	8 ± 3	19 ± 8	^{121}Te	12 ± 1	——[a]
^{71}As	4.2 ± 0.4	11 ± 1	^{125}Xe	25 ± 15	27 ± 16[b]
^{73}Se	2.9 ± 0.3	—[a]	^{127}Xe	16 ± 2	30 ± 3[b]
^{74}As	3.6 ± 0.4	10 ± 1	^{131}Ba	26 ± 3	33 ± 3[b]
^{75}Se	7 ± 4	9 ± 4	^{145}Eu	23 ± 3	28 ± 3
^{75}Br	4 ± 1	14 ± 4	^{147}Eu	18 ± 2	18 ± 2
^{77}Br	9.2 ± 0.6	12 ± 2[b]	^{149}Gd	23 ± 2	25 ± 2
^{81}Rb	5 ± 1	10 ± 3[b]	^{150}Tb	7.8 ± 0.8	—[a]
^{82}Rb	4.9 ± 0.6	—[a]	^{155}Dy	25 ± 3	25 ± 3
^{83}Rb	8.7 ± 0.9	10 ± 1	^{160}Er	15 ± 2	26 ± 3

Table II (cont.)

Product Yields from the Interaction of 25.2 GeV ^{12}C with ^{181}Ta					
Nuclide	Measured Radionuclide Yield (mb)	Isobaric Yield (mb)	Nuclide	Measured Radionuclide Yield (mb)	Isobaric Yield (mb)
^{167}Tm	32 ± 2	55 ± 6	^{171}Lu	39 ± 2	38 ± 4[b]
^{169}Yb	29 ± 5	42 ± 7[b]	^{173}Hf	58 ± 11	65 ± 15
^{169}Lu	42 ± 6	54 ± 8[b]	^{175}Ta	50 ± 7	56 ± 8
^{170}Hf	26 ± 3	43 ± 5	^{176}Ta	66 ± 7	73 ± 7
^{171}Hf	37 ± 5	44 ± 6			

a Mass yield not determined because yields of both members of an isomeric pair not measured.

b The ground state radioactivity of this nuclide when measured at t>> t1/2 (metastable state) effectively sums the yield of metastable and ground states.

Table III

Product Yields from the Interaction of 42 GeV ^{20}C with ^{181}Ta

Nuclide	Measured Radionuclide Yield (mb)	Isobaric Yield (mb)	Nuclide	Measured Radionuclide Yield (mb)	Isobaric Yield (mb)
^{24}Na	23 ± 1	32 ± 3	^{97}Ru	8.0 ± 1.0	12.9 ± 1.6
^{28}Mg	8 ± 2	36 ± 9	^{101m}Rh	6.3 ± 0.6	——[a]
^{42}K	6 ± 2	12 ± 4	^{105}Ag	11 ± 1	11.9 ± 1.1
^{44m}Sc	2.8 ± 0.2	——[a]	^{110m}In	0.8 ± 0.5	——[a]
^{47}Sc	4.9 ± 0.8	10.9 ± 1.8	^{111}In	9.0 ± 0.5	10.2 ± 1.0
^{48}Sc	2.3 ± 0.5	14.3 ± 3.0	^{121}Te	13.7 ± 0.6	19 ± 2
^{48}V	3.4 ± 0.1	13.9 ± 1.4	^{122}Xe	8 ± 1	15 ± 2
^{67}Ga	4.0 ± 1.0	7.5 ± 1.9	^{123}I	11 ± 2	12 ± 2
^{69}Ge	5.5 ± 0.9	12.2 ± 2	^{128}Ba	9 ± 1	12.6 ± 1.4
^{71}As	4.3 ± 0.7	11 ± 2	^{145}Eu	24 ± 2	28 ± 3
^{72}As	5.8 ± 0.4	9.0 ± 0.9	^{147}Gd	18.2 ± 0.6	26.5 ± 2.7
^{74}As	3.1 ± 0.5	8.1 ± 1.3	^{149}Gd	21.7 ± 0.3	21.8 ± 2.2
^{75}Se	14 ± 9	17 ± 11	^{151}Tb	22 ± 4	22.6 ± 4.1
^{87}Y	11.3 ± 0.7	12.3 ± 1.2	^{166}Yb	31 ± 1	40 ± 4
^{87m}Y	7.4 ± 0.9	7.8 ± 1.0	^{169}Yb	38 ± 7	55 ± 10
^{89}Zr	8.7 ± 0.8	9.9 ± 0.9	^{171}Lu	36 ± 5	34 ± 5
^{90}Nb	4.3 ± 0.7	8.0 ± 1.3	^{173}Hf	38 ± 6	41 ± 7
^{95}Tc	7.0 ± 1.0	9.9 ± 1.4	^{176}Ta	22 ± 3	24 ± 3

a Isobaric yield not computed because substantial fraction of yield in unobserved member of isomeric pair.

Table IV

Total Residue Cross Sections

Reaction	Ecm A	Integrated Cross Section A ≥ 60	Fission Correction	Total Residue Cross Section $^{20}Ne + ^{181}Ta$	Ref.
$^{20}Ne + ^{197}Au$	7.5	3179	1432[a]	1709	12
$^{16}O + ^{197}Au$	11.1	3278	1036[a]	2352	11
$^{16}O + ^{197}Au$	17.1	4302	1180[a]	3281	11
$^{12}C + ^{196}Au$	42.8	3791	722[a]	3618	11
$^{12}C + ^{197}Au$	79.0	3304	364[a]	3511	11
$^{12}C + ^{181}Ta$	234.5	2285	60[b]	2721	this work
$^{20}Ne + ^{181}Ta$	360.2	2680	60[b]	2620	7
$^{12}C + ^{197}Au$	377.0	2780	250[b]	3020	19
$^{20}Ne + ^{181}Ta$	1891.0	2250	55[b]	2195	this work
$^{12}C + ^{181}Ta$	1969.4	2578	50[b]	3079	this work

a. Estimated from isobaric yield distribution by assuming all events in central "hump" in distribution are fission events

b. Estimated from measured [17] fission cross sections for $^{197}Au + ^{14}N$ and systematics [18] of the variation of Γ_f in going from ^{197}Au to ^{181}Ta.

References

* Present address: Rockwell International, Energy Systems Group, Golden, CO 80401

+ Present address: Los Alamos National Laboratory, Los Alamos, NM 87545

1. DeVries, R., Peng, J. C., Phys. Rev. Letter. 43, 1373 (1979).

2. DeVries, R., Peng, J. C., Phys. Rev. C22, 1055 (1980).

3. Peng, J. C. DeVries, R. M., and Di Giacomo, N. J., Phys. Lett. 98B, 244 (1981).

4. Buenerd, M., Pinston, J., Cole, J., Guet, C., Lebrun, D., Loiseaux, J.M., Martin, P., Monard, E., Mougey, J., Nifenecker, H., Ost, R., Perrin, P., Ristori, Ch., de Saintignon, P., Schussler, F., Carlen, L., Gustaffson, H. A., Jakobsson, B., Johansson, T., Jonsson, G., Krumlinde, J., Otterlund, I., Ryde, H., Schroder, B., Tibell, G., Bondorf, J.B., Nielson, O.B., Phys Lett. 102B, 242 (1981).

5. Grabez, B., Beckman, R., Vater, P., Brandt, R., Nucl. Instr. Meth. (to be published), see also GSI - Scientific Report 1983, p 30.

6. Morrissey, D.J., Lee, D., Otto, R.J., Seaborg, G. T., Nucl. Instr. Meth. 158, 499 (1978).

7. Morrissey, D. J., Loveland, W., de Saint-Simon, M., Seaborg, G. T., Phys. Rev. C21, 1783 (1980).

8. Aleklett, K., Morrissey, D. J., Loveland, W., McGaughey, P. L., Seaborg, G. T., Phys. Rev C23, 1044 (1981).

9. Wilkins, B.D., Kaufman, S.B., Steinberg, E. P., Urbon, J.A., Henderson, D. J., Phys. Rev. Lett. 43, 1080 (1979).

10. Warwick, A. I., Wieman, H. H., Gutbrod, H. H., Maier, M. R., Peter, J., Ritter, H. G., Stelzer, H., Weik, F., Freedman, M., Henderson, D. J., Kaufman, S. B., Steinberg, E. P., Wilkins, B. D., Phys. Rev. C27, 1083 (1983).

11. Loveland, W., Aleklett, K., McGaughey, P.L., Moody, K.J., McFarland, R.M., Kraus, Jr., R.H., Seaborg, G. T., Phys. Rev. C. (submitted for publication).

12. I. Binder, Lawrence Berkeley Laboratory Report LBL - 6526, July, 1977, (unpublished).

13. P. J. Karol, Phys. Rev. C11, 1203 (1975).

14. Heckman, H. H., Greiner, D. E., Lindstrom, P. J., Shue, H., Phys. Rev. C17, 1735 (1978).

15. Videbaek, F., Goldstein, R. B., Grodzins, L., Steadman, S. G., Belote, T.A., Garrett, J.D., Phys. Rev. C15, 954 (1977).

16. Townsend, L. W., Wilson, J. W., Bidasaria, H. B., Can. J. Phys. 60, 1514 (1982); see also NASA Technical Paper 2138, April, 1983.

17. Katcoff, S., Hudis, J., Phys. Rev. C14, 618 (1976).

18. Vandenbosch, R., Huizenga, J. R., Nuclear Fission, (Academic, New York, 1973)

19. Kaufman, S. B., Steinberg, E. P., Wilkens, B.D., Henderson, D. J., Phys. Rev. C22, 1897, (1980).

Figure Captions

1. The charge dispersion curves for products from the reaction of 3.0 GeV ^{12}C with ^{181}Ta are shown for various mass regions. Isomeric yields are indicated by triangles.
2. The charge dispersion curves for products from the reaction of 25.2 GeV ^{12}C with ^{181}Ta.
3. The charge dispersion curves for products from the reaction of 42.0 GeV ^{20}Ne with ^{181}Ta.
4. The dependence of the most probable primary fragment charge, Zp, upon product mass number A for the reaction systems studied in this work.
5. The fragment isobaric yield distributions for the cases studied in this work.
6. The variation of the deduced lower limits of the total reaction cross section, $\sigma_R^<$, as a function of the projectile energy. Also shown are other measurements of σ_R and two optical model calculations of σ_R.

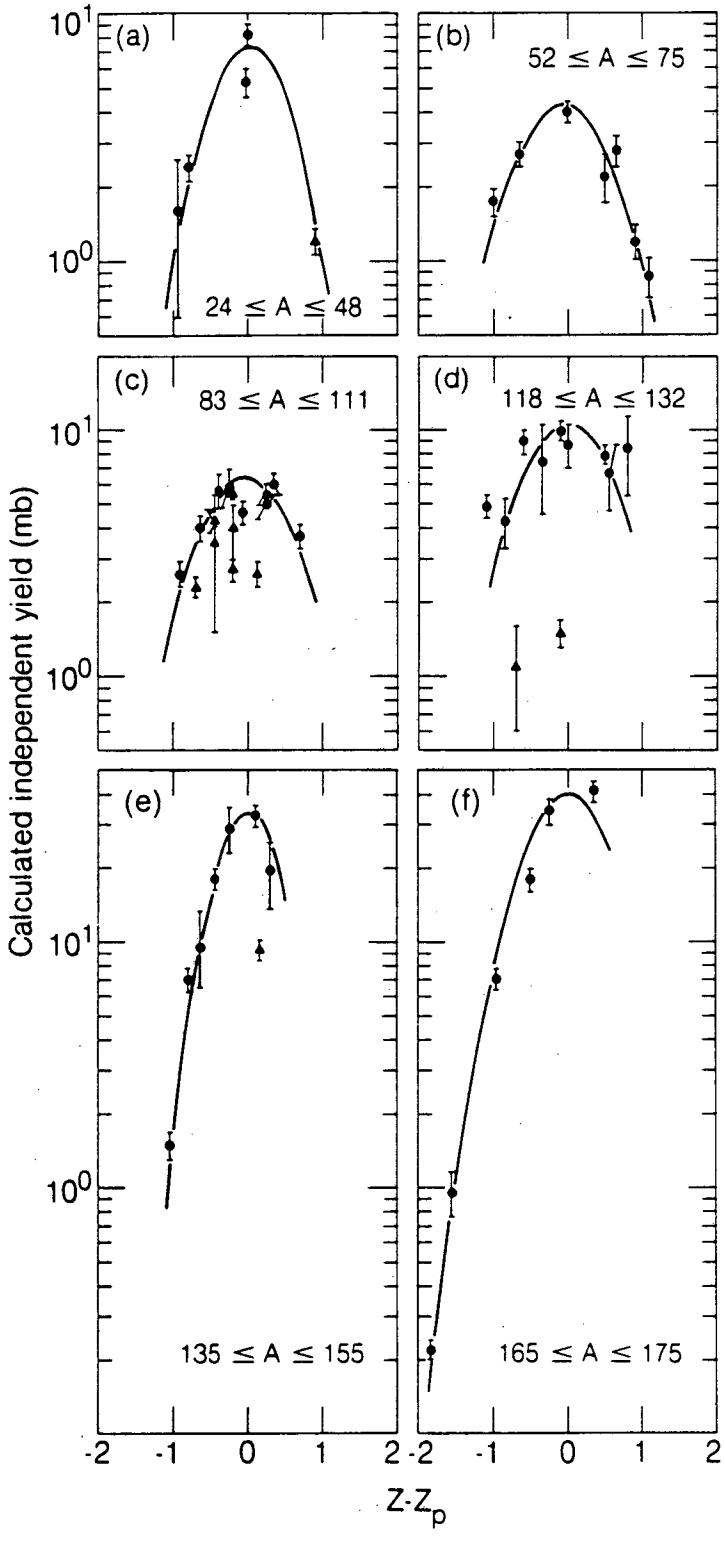
(a)
24 ≤ A ≤ 48
(b)
52 ≤ A ≤ 75
(c)
83 ≤ A ≤ 111
(d)
118 ≤ A ≤ 132
(e)
135 ≤ A ≤ 155
(f)
165 ≤ A ≤ 175
Calculated independent yield (mb)
Z-Z_p
XBL 836-951

Fig. 1

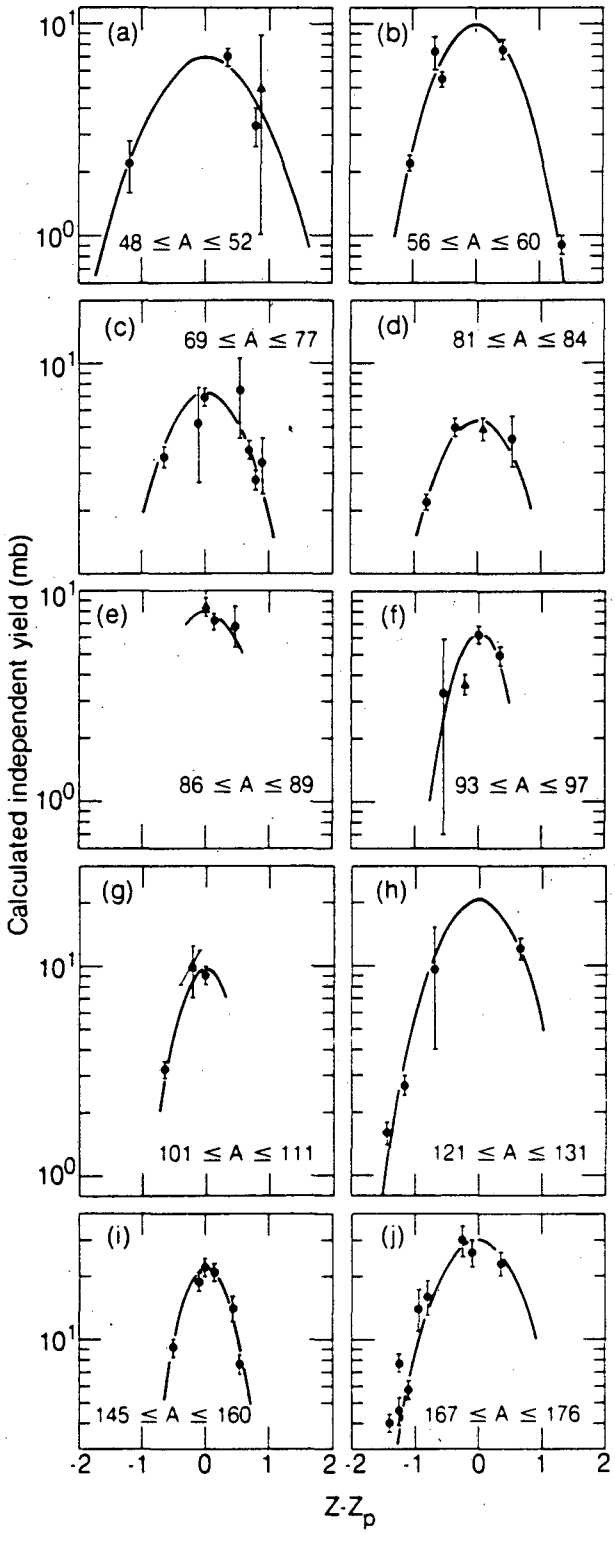
(a)
48 ≤ A ≤ 52
(b)
56 ≤ A ≤ 60
(c)
69 ≤ A ≤ 77
(d)
81 ≤ A ≤ 84
(e)
86 ≤ A ≤ 89
(f)
93 ≤ A ≤ 97
(g)
101 ≤ A ≤ 111
(h)
121 ≤ A ≤ 131
(i)
145 ≤ A ≤ 160
(j)
167 ≤ A ≤ 176
Calculated independent yield (mb)
Z-Z_p
XBL 836-952

Fig. 2

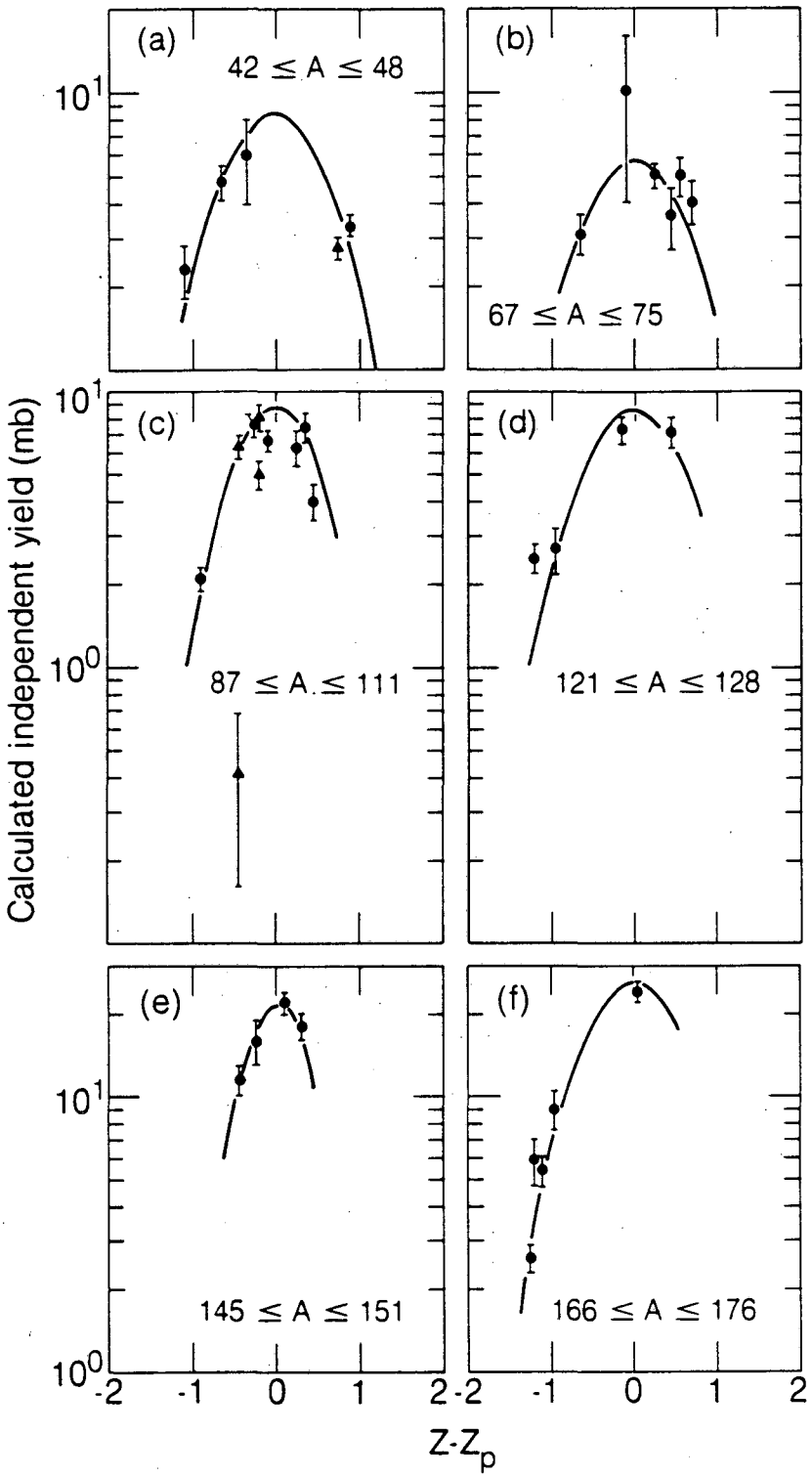
(a)
42 ≤ A ≤ 48
(b)
67 ≤ A ≤ 75
(c)
87 ≤ A ≤ 111
(d)
121 ≤ A ≤ 128
(e)
145 ≤ A ≤ 151
(f)
166 ≤ A ≤ 176
Calculated independent yield (mb)
Z-Z_p
XBL 836-950

Fig. 3

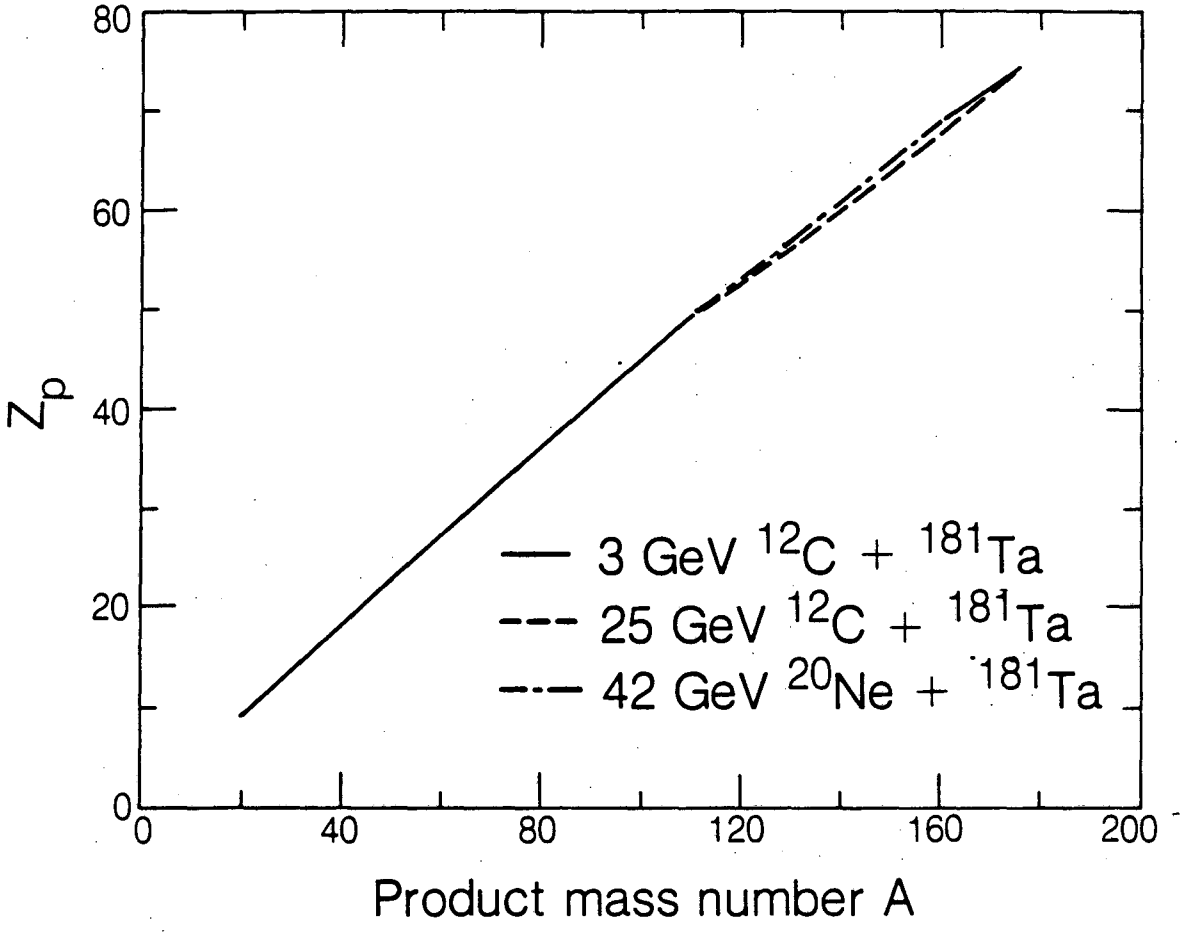

XBL 836-954

Fig. 4

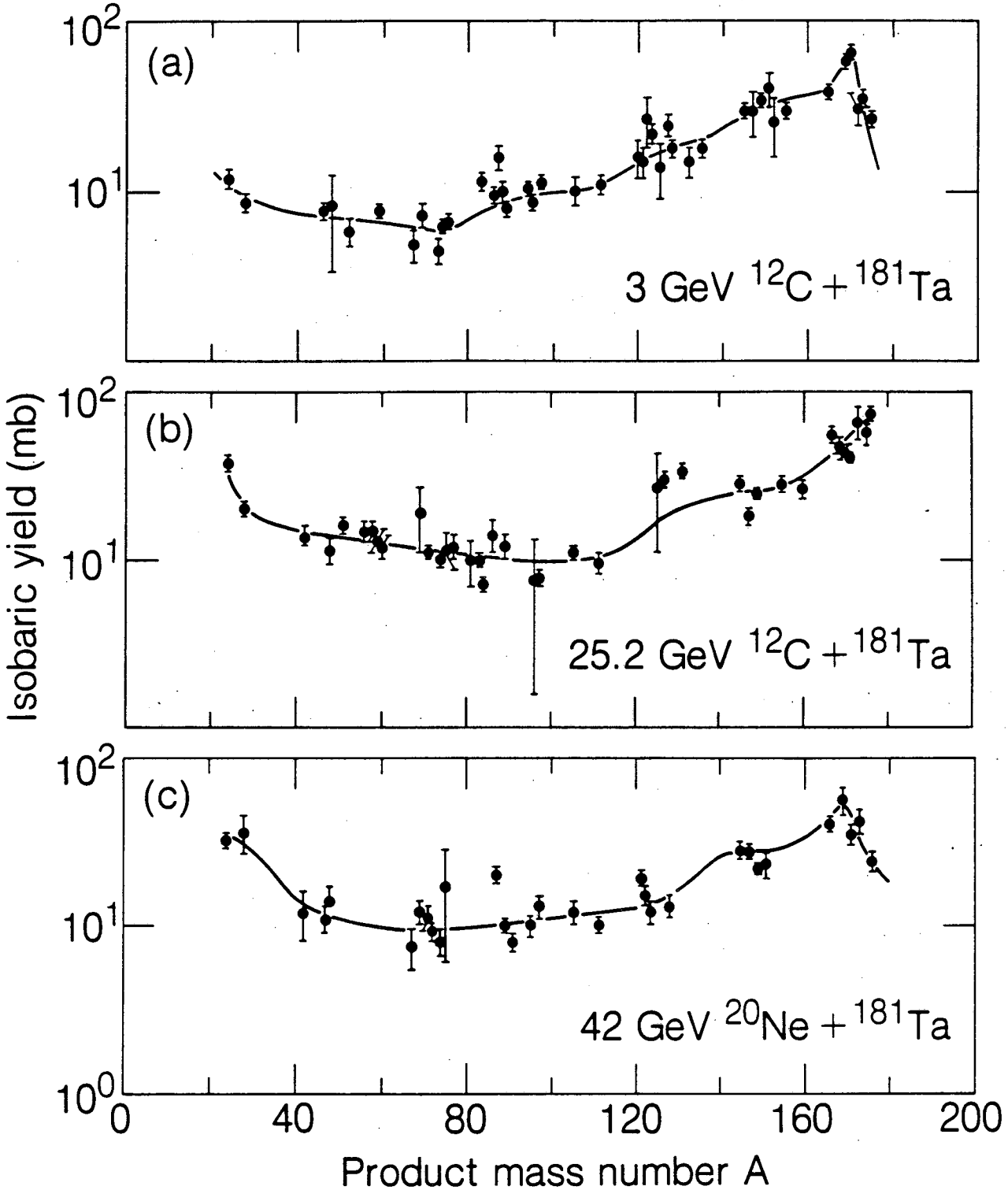

XBL 836-955

Fig. 5

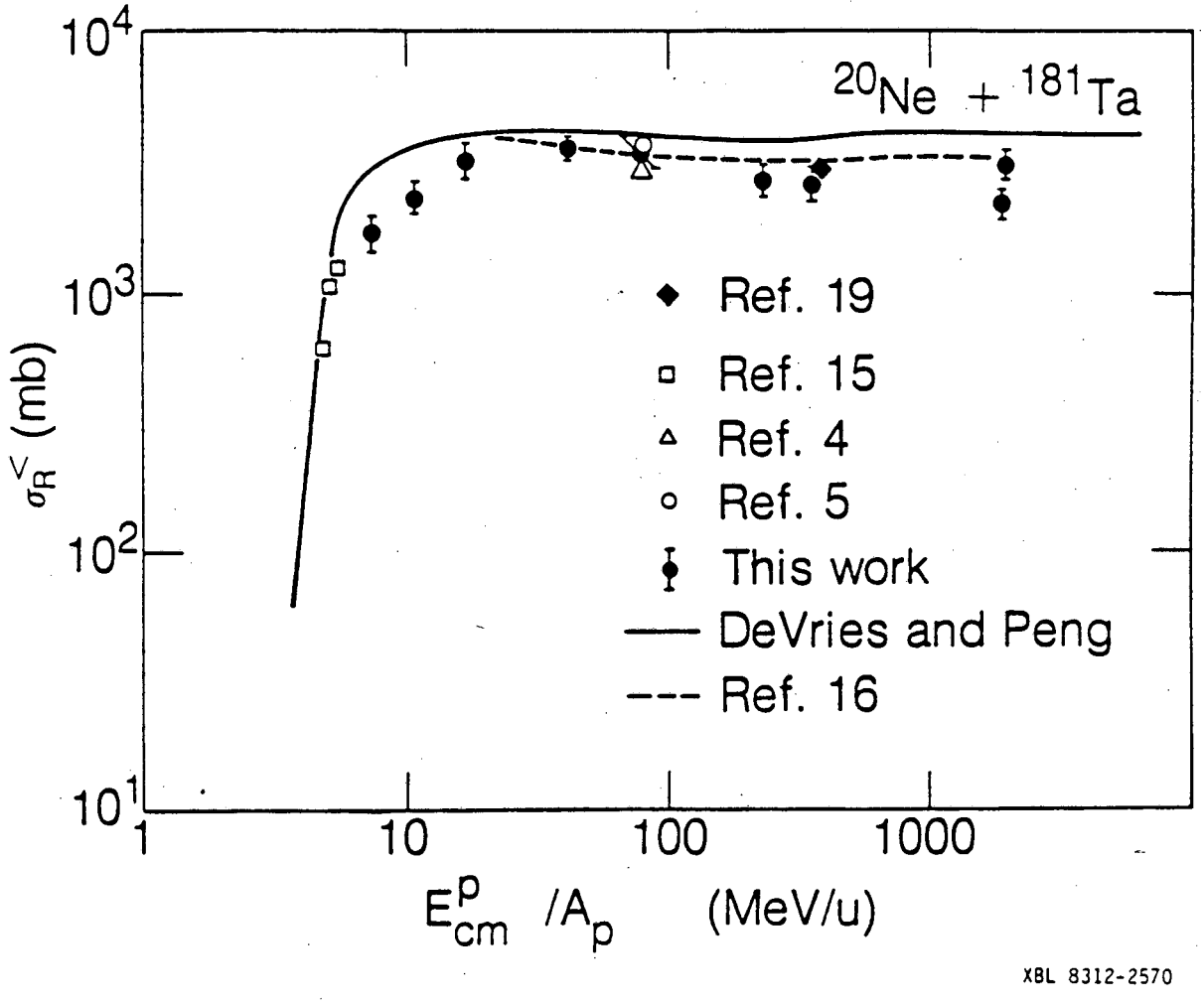
$^{20}Ne + ^{181}Ta$
Ref. 19
Ref. 15
Ref. 4
Ref. 5
This work
DeVries and Peng
Ref. 16
σ_R^V (mb)
E^p_{cm}/A_p (MeV/u)
10^4
10^3
10^2
10^1
1
10
100
1000
XBL 8312-2570

Fig. 6

TECHNICAL INFORMATION DEPARTMENT
LAWRENCE BERKELEY LABORATORY
UNIVERSITY OF CALIFORNIA
BERKELEY, CALIFORNIA 94720